Draft version 0.0

ATLAS NOTE

March 30, 2015

Searches for the exclusive double diffractive Higgs

L. Feremenga[a], L. Nodulman[b], C. C. Chau[c], S. Chekanov[b], J. Griffiths[a], B. Blair[b], J. Yu[a]

[a] *University of Texas at Arlington*
[b] *Argonne National Laboratory*
[c] *University of Toronto*

Abstract

The exclusive Higgs could be a clean channel to study Higgs properties. The most popular theoretical model for the exclusive Higgs predicts a total cross section of 3 fb at LHC 8 TeV collision energy. This note summarizes a search for the exclusive Higgs boson using ATLAS 8 TeV data, using the $H \rightarrow WW^* \rightarrow lvlv$ decay channel with different flavor leptons in the final state. Selection criteria were developed to isolate exclusive processes from inclusive processes. Selection criteria that isolate Higgs-like events that were inherited from previous Higgs searches were also utilized. A limit of 770 fb on the total cross section of the exclusive Higgs production was obtained.

Contents

1 Introduction

Theoretical studies that attempt to estimate the event rates for the exclusive diffractive Higgs boson at the LHC have been previously preformed [1] [2]. In these studies rapidity gaps between the Higgs decay products and the outgoing protons play the most active role. At high luminosities however, these rapidity gaps are corrupted by pileup events and can hardly be used to separate exclusive processes from inclusive processes. This result has diverted attention to ATLAS' ALFA detectors which could be used as taggers for the outgoing protons. A search for an exclusive pion pair has been used to test the feasibility of these ALFA detectors [3].

The most recent experimental searches for exclusive events were done at 7 TeV by ATLAS and CMS [4] [5] [6]. Here isolated lepton pairs from QED production were searched for by looking for isolated vertices with only two lepton tracks; no rapidity gaps or proton tagging was used. At 8 TeV however the strategy of looking for vertices with only two tracks was found to be inefficient using exclusive $H \rightarrow W^+W^- \rightarrow l^+\nu l^-\nu$ Monte Carlo samples. Feasibility studies by the tracking group confirmed this inefficiency and demonstrated that vertexing algorithms at 8 TeV tend to generously associate tracks with vertices. This obviously contaminates the exclusive signal.

In this note a search for exclusive events using an algorithm that utilizes neither vertexing, rapidity gaps nor proton tagging is presented. Exclusive $H \rightarrow W^+W^- \rightarrow l^+\nu l^-\nu$ events survival rate is improved. The note is organized as follows: Section 2 describes briefly the physics of exclusive diffractive Higgs production. The Khoze Martin Ryskin (KMR) and CHIDe models are described and their sources of theoretical systematic uncertainties are outlined. A discussion of the Monte Carlo (MC) sample used to study the signal and a list of backgrounds and their MC is outlined as well in this section. Section 3 describes the object and event selection. Section 4 introduces the algorithm for selecting exclusive events. Here the signal survival rate is quoted and the exclusivity cut is tested in data. Section 7 estimates the expected number of signal events versus background events in the signal region.

2 Theory

The Feynman diagram shown in Figure 1 describes the production of the exclusive double diffractive Higgs boson. In this QCD mechanism two gluons interact through a top quark loop to form the Higgs boson while a third gluon is exchanged to keep the protons color neutral and hence intact. Calculations for this process have been studied extensively. The most popular calculations are performed by the KMR and the CHIDe models, which differ very slightly and predict similar cross sections [7][8]. Both models introduce the proton impact factor through the skewed unintegrated gluon density [9], calculate the probability of additional gluon density using the Sudakov form factor [10]. Both models also take into account the probability of soft interaction between the outgoing protons. This interaction tends to destroy the intactness of the outgoing protons, and hence destroys the rapidity gaps associated with exclusive processes. There are two main differences between the KMR and the CHIDe models: CHIDe uses different limits to compute the Sudakov factor and also includes an additional K-factor to introduce some NLO corrections. As a result, KMR predicts a higher cross section for the exclusive double diffractive Higgs than CHIDe. For a 125GeV Higgs KMR predicts 3 fb at $\sqrt{s}$ = 8TeV [7].

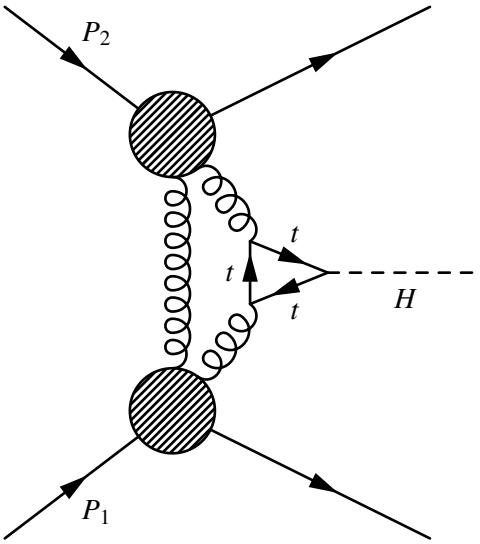

Figure 1:

There are two main sources of theoretical systematic uncertainties that have to be studied: upper and lower Sudakov form factor scales, unintegrated gluon densities. Uncertainties associated with the rapidity gap survival probability were originally studied for the Tevatron and subsequently for the LHC [11]. In this analysis we will not use rapidity gaps for event selection so uncertainties from rapidity gaps are estimated to be minimal.

2.1 Signal and Background Models

Both the KMR and CHIDe models are implemented in the Forward Physics Monte Carlo (FPMC). For signal we generate exclusive $H \rightarrow WW^* \rightarrow lvlv$ within KMR using FPMC and shower with Herwig. The results are then run through the full simulation of the ATLAS detector. This signal is characterized by very little activity around the dileptons.

Background processes can be separated into exclusive and inclusive. Inclusive backgrounds are those in which the two protons dissociate and the by-products are detected by the ATLAS detector. All these backgrounds are estimated using several MC samples except the W+jets background, in which the jet is misidentified as a lepton. A tested and verified data-driven method is used to estimate W+jets. See

Section VIC from Ref. [12] for a detailed description of this method. The rest of the backgrounds are listed in Table 1.

The Z/γ^*+jets background is dominated by $Z/\gamma^* \rightarrow \tau\tau$+jets in which the taus decay leptonically to a different flavor channel. If the jets are misidentified as $E_{\mathrm{T}}^{\mathrm{miss}}$ the two leptons from the final state would fake the $H \rightarrow WW^* \rightarrow lvlv$ signature. Of the $Z/\gamma^* \rightarrow \tau\tau$+jets processes, the 0-jet process contributes the most signal contamination because it has the least activity around the dilepton system. These processes are generated with Alpgen and showered with Herwig.

$t\bar{t}$ is a background to the Higgs signature when the two top quarks decay to a WW system and a pair of b jets. MC@NLO is used to generate this process and Jimmy is used for showering. A single top quark is also a background process because a b jet can be misidentified as a lepton. Powheg is used to generate single top events and the showering is done with Pythia.

Because the signal is produced through gluon exchanges (See Figure 1), ggF Higgs is a background. ggF Higgs is generated with Powheg and showered with Pythia8. Apart from the intensity of activity about the dilepton system, the kinematics of ggF Higgs is identical to that of the exclusive Higgs.

Another irreducible inclusive background is a pair of W bosons. It is refered to as *inclusive WW* in this note. The final decay products are identical to signal so kinematic distributions are used to separate this background from signal. This is modelled by Powheg and Pythia.

The rest of the inclusive backgrounds will be referred in this note as *Other VV*. This is because they all constitute a pair of vector bosons. These are $W\gamma$, $W\gamma^*$, $Z\gamma$, $Z\gamma^*$, ZZ, WZ and double-parton interaction (DPI). The MC samples for these processes are listed in Table 1.

The main contribution to the exclusive background is the exclusive boson pair. Exclusive lepton pairs have a very small cross section compared to exclusive boson pairs. Regardless, they are also considered in this study. In both cases photons are exchanged, in contrast to gluons exchanged in the exclusive Higgs production. Three diagrams contribute to the exclusive boson pairs. Figure **??** shows the three different diagrams. In a purely elastic process none of the two protons dissociate during the collision. The intact protons vanish along the beamline and the fiducial region sees only the WW decay products. In a Single Dissociative (SD) process one of the protons dissociate, but the remnants of the dissociation vanish along the beamline. A Double Dissociative (DD) process is similar to an inclusive process, but the proton remnants disappear along the beamline. The three processes have identical kinematic process, so it is impossible to distinguish them. Only the purely elastic diagram is modeled by the available MC, Herwig++. Data driven methods are used to estimate the SD and DD contributions.

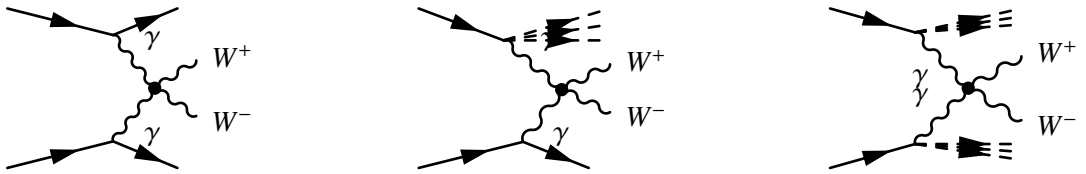

Figure 2: Diagrams that contribute to the exclusive WW processes. [Left] A purely elastice process. No proton dissociates and the two protons vanish along the beamline. [Middle] A single dissociative (SD) process. One proton dissociates but vanishes along the beamline. [Right] A double dissociative (DD) process. Both protons dissociate but the remnants vanish along the beamline. Rapidity gaps are present in all three diagrams and the kinematic distributions are identical, so they are indistinguishable.

2.2 Data Samples

All the data used is from the ATLAS 2012 8 TeV run and sums up to a total integrated luminosity of 20.3 fb^{-1}. The D3PDs used are the most up-to-date and are identified with the tag p1328/p1329. The integrated luminosity is obtained through an ATLAS luminosity calculator [13].

Inclusive Background	Exclusive Background
Drell Yan Z/γ^*+jets (Alpgen+Herwig)	WW (Herwig++)
Wγ +jets (Alpgen+Jimmy)	l^+l^- (Herwig++)
WZ, WW, ZZ, ggF Higgs (Powheg+Pythia8)	
$t\bar{t}$ (MC@NLO+Jimmy)	
single top (AcerMC+Pythia)	
Zγ +jets (Sherpa)	

Table 1: Background samples used.

3 Event and Object Selection

At preselection, events must pass an OR of `EF_e24vhi_medium1`, `EF_mu24i_tight`, `EF_e60_medium1`, `EF_mu36_tight`, `EF_e12Tvh_medium1_mu8`, `EF_mu18_tight_mu8_EFFS` and `EF_2e12Tvh_loose1` to get considered for analysis. They must also have exactly two leptons with $p_{\mathrm{T}} > 15$ GeV. A reconstructed primary vertex is not required to have a minimum number of tracks associated with it. All other preselection cuts are identical to those used for the $H \to WW^* \to \ell^+\ell^-$ study in Ref. [12].

The electron identification criteria closely follows the standard $H \to WW^* \to \ell^+\ell^-$ selection which relies on a likelihood-based method to identify electrons from electromagnetic (EM) showers and Inner Detector (ID) tracks. A more detailed description of this method can be found in Ref. [12]. EM showers and ID tracks are required to have $p_{\mathrm{T}} > 15$ GeVand lie in pseudorapidity less than 2.47 and out of the detector crack ([1.37,1.52]). Electron candidates with $15 < p_{\mathrm{T}} < 25$ GeVhave to satisfy the very tight likelihood requirement and those with $p_{\mathrm{T}} > 25$ GeVhave to satisfy the medium likelihood requirement. This is because the latter are less likely to be misidentified objects. Calorimeter isolation is also imposed on electron objects by considering the energy deposited in a cone of $\Delta R = 0.3$ around the electron object cluster. Track isolation is also considered by taking the sum p_{T} of all the tracks with $p_{\mathrm{T}} > 400$ MeV within a cone of size $\Delta R = 0.3$. To separate these electron objects from prompt electrons, impact parameter variables are used. The transverse impact parameter d_0 is required to satisfy $|d_0|/\sigma_{d_0} < 3.0$ where σ_{d_0} is the uncertainty on d_0. The longitudinal impact parameter must satisy $|z_0 \sin\theta| < 0.04$ mm. This improves the probability of selecting leptons that originate from the primary vertex. Figure 3 shows the p_{T} and η distributions for electrons that pass all these requirements.

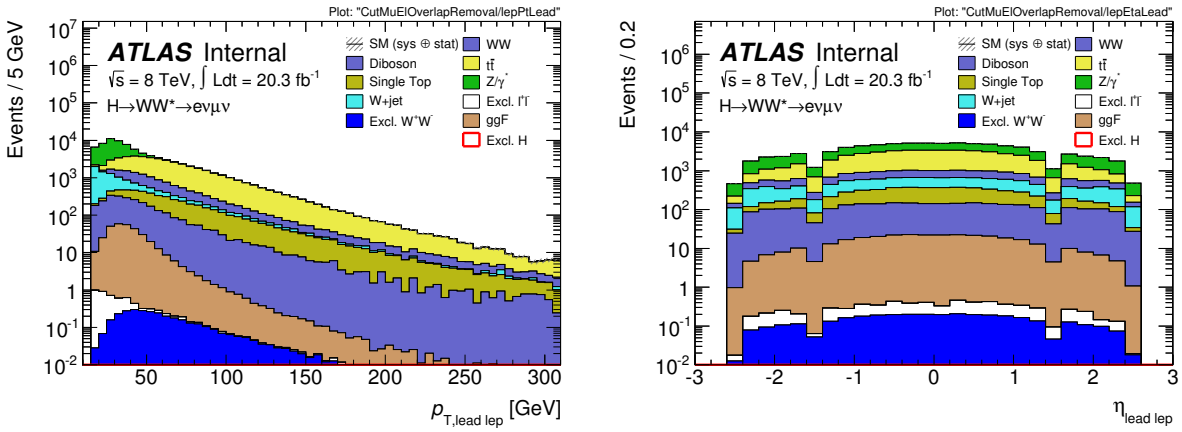

Figure 3: p_{T} [left] and η [right] distributions for electron candidates that pass all the electron selection criteria.

Candidates for muon objects should be objects with matched hits from the ID and the Muon Spectrometer (MS). The algorithms that match ID tracks to MS tracks are described in detail in Ref. [14]. These objects are further required to have $p_{\mathrm{T}} > 15$ GeV and must lie within pseudorapidity of 2.47. Muon selection is insensitive to the calorimeter crack that covers $1.37 < |\eta| < 1.52$. That is the reason why the only η requirement imposed on muon candidates is for them to lie within 2.47 in η. The sum of the pixel hits and dead sensors should be at least 1. The sum of sct hits and dead sensors should also be at least 5. This ensures that the ID track is a good candidate for matching with an MS track. Track isolation criteria is identical to that imposed on electron candidates. No calorimeter isolation is required on muons. Figure 4 shows the p_{T} and η distribution of muon candidates that pass all the muon selection criteria.

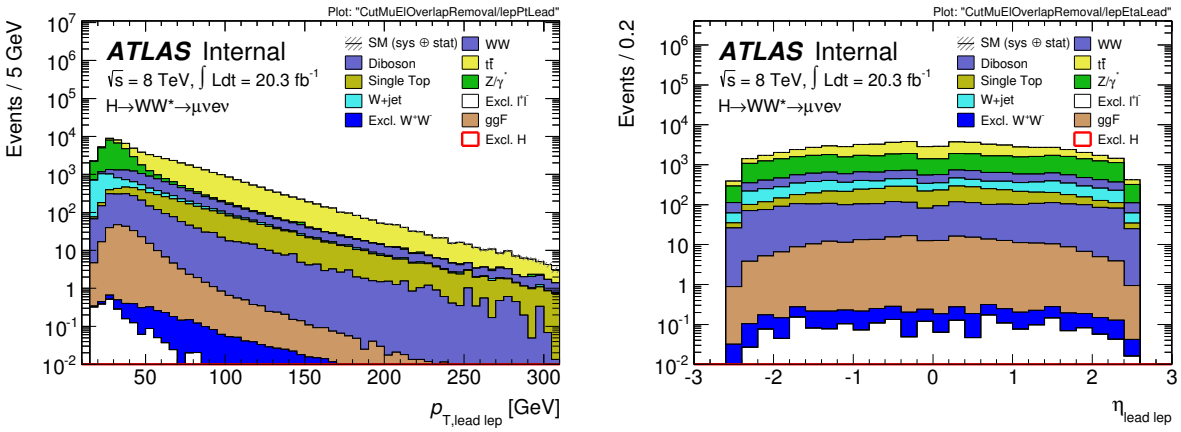

Figure 4: p_{T} [left] and η [right] distributions for muon candidates that pass all the muon selection criteria.

Electrons and muons can sometimes be very close in $\eta - \phi$ space. If an electron and a muon are within $\Delta R < 0.1$, where $\Delta R = \sqrt{\eta^2 + \phi^2}$, the electron is removed and the muon is kept. This is motivated by the theory that the muon would have undergone bremsstrahlung. If an electron track is seen in the muon spectrometer, it is removed. If two electrons are within $\Delta R < 0.1$, the electron with higher E_{T} is kept and the other one is discarded. We will refer to this process as *Electron-Muon Removal* in this note.

Tracks are required to have at least 1 pixel hit and at least 4 sct hits. The minimum p_{T} that achieved on these tracks is 400 MeV. Availability of low-p_{T} tracks increases rejection on QCD multijets and improves the signal survival efficiency. Reasons for this assertion will become clearer after the exclusivity selection criteria is discussed in detail in section 4. Track candidates are also required to be within $|\eta| < 2.47$. This is in line with the lepton angular selection criteria. Figure 5 shows the number of tracks that pass this criteria.

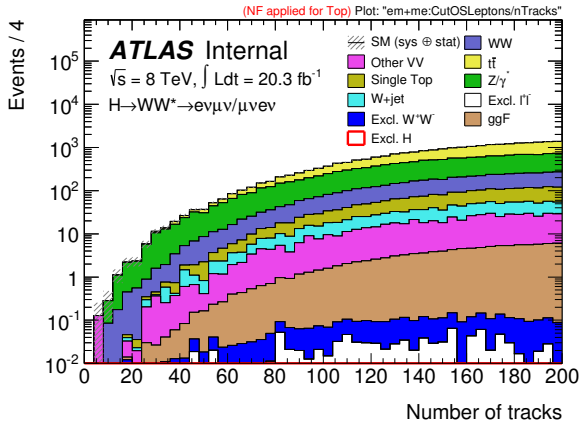

Figure 5: Number of track candidates that pass the track selection criteria.

The signal region for events that pass the pre-selection criteria is carefully designed to select events that have Higgs-like kinematic properties. An exclusivity requirement is further imposed on these events to select events with additional exclusivity-like kinematic properties. The lepton with higher p_{T} (of the two selected leptons) is required to have $p_{\mathrm{T}} > 25$ GeV. This will be refered to as the 'leading lepton'. The second lepton, with lower p_{T} is required to have $p_{\mathrm{T}} > 15$ GeV. It will be refered to as the 'sub-leading lepton'. The high p_{T} selection on the leptons is meant to reduce W+jets and QCD multi-jets backgrounds, where low-p_{T} jets are mis-identified as leptons. To exploit the fact that the SM Higgs is

neutral, the leading and sub-leading leptons are required to be of opposite sign. This cut will be refered to as 'OS Leptons' in this note.

The invariant mass of the dilepton system m_{ll}, is demanded to be fall within 10 GeV and 55 GeV. The reason for a lower bound is that some of the backgrounds such at Z+jets are not modelled correctly at low m_{ll}. In this analysis only Z+jets MC samples generated at $m_{ll} > 10$ GeV are used. Figure 6 shows the m_{ll} distribution for events that pass the preselection cuts, lepton p_{T} cuts and the opposite sign requirement on the leptons. The $m_{ll} > 10$ GeV cut yields a signal survival efficiency of 98%. Figure 6 also justifies an upper bound on m_{ll} for Higgs events. Since the Higgs boson is of spin zero, m_{ll} tends to peak at lower values than for the WW backgrounds. A $m_{ll} < 55$ GeV cut rejects 75% of inclusive WW background and keeps 86% of signal.

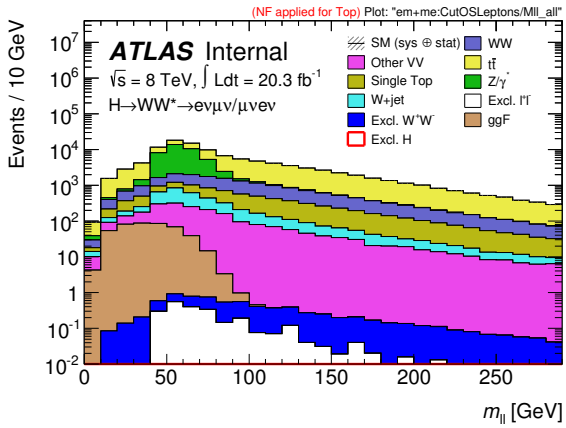

Figure 6: m_{ll} distribution for signal (scaled by 10^4) and relevant backgrounds for events that pass preselection, lepton p_{T}, and OS lepton cuts. Z+jets are not well modelled for $m_{ll} < 10$ GeV, so we consider events with $m_{ll} > 10$ GeV. Signal survival after this cut is 98%. An $m_{ll} < 55$ GeV cut further rejects 75% of WW background while keeping 86% of signal.

The neutrinos in the signal final state are identified by a momentum imbalance in the detector. This imbalance is quantified by the variable 'missing transverse momentum', $E_{\mathrm{T}}^{\mathrm{miss}}$ that is calculated as

$$E_{\mathrm{T}}^{\mathrm{miss}} = -\left(\sum_{selected} p_{\mathrm{T}} + \sum_{soft} p_{\mathrm{T}} \right) \tag{1}$$

where $\sum_{selected} p_{\mathrm{T}}$ is the vectorial sum of p_{T} from all the objects identified by ATLAS identification algorithms, such as leptons, photons and jets. In this analysis these objects are required to have $p_{\mathrm{T}} > 20$ GeV. $\sum_{selected} p_{\mathrm{T}}$ is the vectorial sum of p_{T} from all other objects that have low values of p_{T}, extracted from tracks with $p_{\mathrm{T}} > 0.5$ GeV that originate from the primary vertex. Both $E_{\mathrm{T}}^{\mathrm{miss}}$and its relative direction to leptons and jets are effective variables in rejecting Drell-Yan $\tau^+\tau^-$ background, where $E_{\mathrm{T}}^{\mathrm{miss}}$ aligns with a final state lepton. A special variable, $E_{\mathrm{T,rel}}^{\mathrm{miss}}$(see Ref. [12] for a more detailed description of this variable) is used to quantify how close in the transverse plane $E_{\mathrm{T}}^{\mathrm{miss}}$ is to leptons and jets:

$$E_{\mathrm{T,rel}}^{\mathrm{miss}} = \begin{cases} E_{\mathrm{T}}^{\mathrm{miss}} \sin \Delta\phi_{near} & \text{if } \Delta\phi_{near} < \pi/2 \\ E_{\mathrm{T}}^{\mathrm{miss}} & \text{otherwise,} \end{cases} \tag{2}$$

where $\Delta\phi_{near}$ is the azimuthal separation of $E_{\mathrm{T}}^{\mathrm{miss}}$ and the nearest high-p_{T}jet or lepton. Figure **??** shows $E_{\mathrm{T}}^{\mathrm{miss}}$ [left] and $E_{\mathrm{T,rel}}^{\mathrm{miss}}$ [right] for events that pass the pre-selection, electron-muon removal cuts, lepton p_{T} cuts, the 10 GeV m_{ll}minimum requirement and the opposite sign requirement on the leptons.

For events with 0 or 1 jets, we demand $E_{\mathrm{T}}^{\mathrm{miss}} > 20$ GeV. For events with 2 or more jets, we demand $E_{\mathrm{T,rel}}^{\mathrm{miss}} > 25$ GeV. These criteria are discussed in detail, with supporting $E_{\mathrm{T}}^{\mathrm{miss}}$ and $E_{\mathrm{T,rel}}^{\mathrm{miss}}$ distributions, in Ref. [12]. As a result Drell-Yan $\tau^+\tau^-$ and backgrounds with a misidentified lepton are reduced.

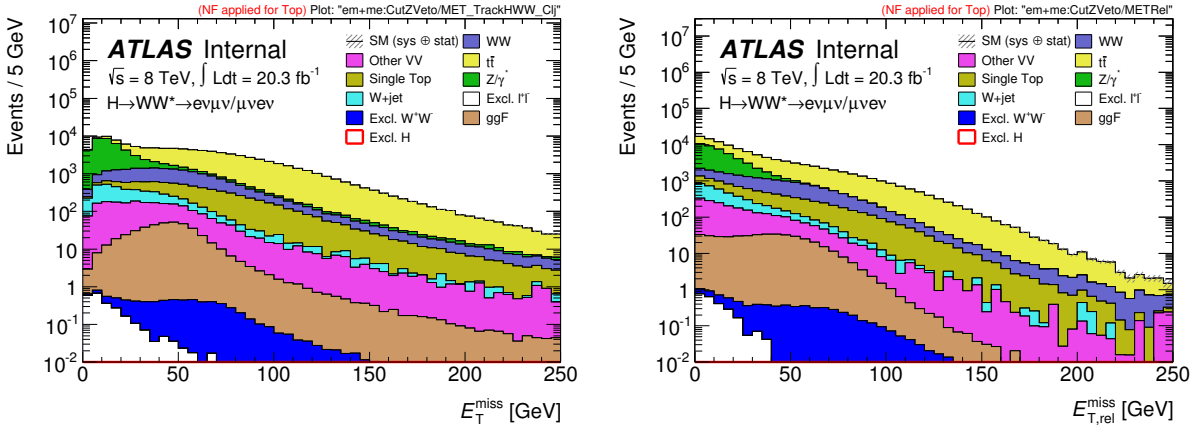

Figure 7: $E_{\mathrm{T}}^{\mathrm{miss}}$ [left] and $E_{\mathrm{T,rel}}^{\mathrm{miss}}$ [right] for events that pass pre-selection, electron-muon removal, lepton p_{T}, $m_{ll} > 10$ GeV cut and the opposite sign requirement on the leptons. These variables are crucial in reducing Drell-Yan $\tau^+\tau^-$ and those backgrounds that have a misidentified lepton.

To ensure that $E_{\mathrm{T}}^{\mathrm{miss}}$ is not mismeasured, it is important to establish some separation in ϕ between $E_{\mathrm{T}}^{\mathrm{miss}}$ and the dilepton system. The variable $\Delta\phi_{\ell\ell,MET}$ shown in Figure 8 quantifies this separation. We demand $\Delta\phi_{\ell\ell,MET} > \pi/2$ for the signal region. As shown in Figure 8 this requirement suppresses W+jets and Drell-Yan $\tau^+\tau^-$. p_T^{ll} is also used in this analysis to suppress $\tau^+\tau^-$ Drell-Yan backgrounds. The right plot in Figure 8 shows that $Z/\gamma^* \to \tau^+\tau^-$ tends to have low p_{T}. In this analysis we demand $p_T^{ll} > 30$ GeV and keep 90% of signal.

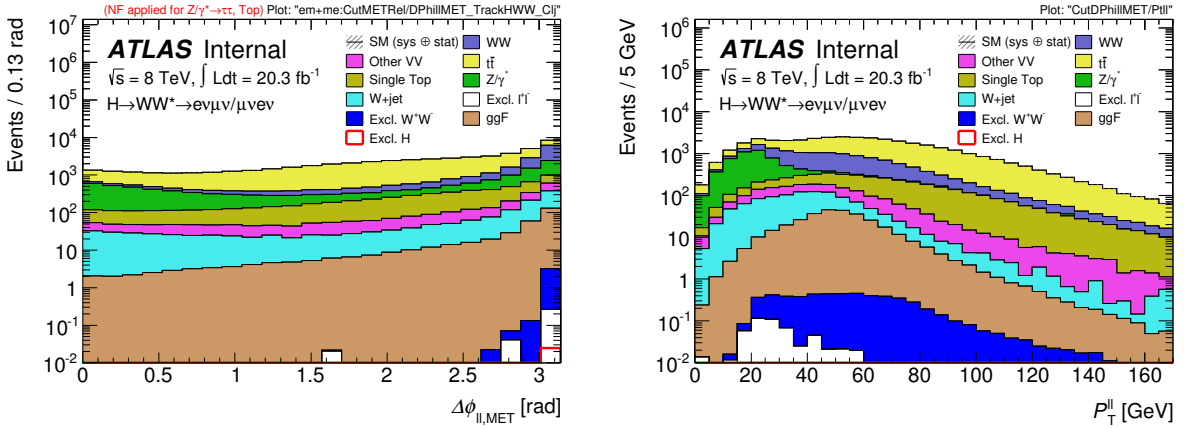

Figure 8: $\Delta\phi_{\ell\ell,MET}$ [left] quantifies separation in ϕ-space between $E_{\mathrm{T}}^{\mathrm{miss}}$ and the dilepton system. This is important to suppress mismeasurement of $E_{\mathrm{T}}^{\mathrm{miss}}$ and further suppresses W+jets and Drell-Yan $\tau^+\tau^-$ backgrounds. p_T^{ll} [right] is also a good variable for suppressing Drell-Yan $\tau^+\tau^-$. Signal region demands $p_T^{ll} > 30$ GeV which keeps 90% of the signal.

The angular separation in ϕ between the two leptons $\Delta\phi_{ll}$ which is closely related to m_{ll} is used to reduce the WW continuum. We require that $\Delta\phi_{ll} > 1.8$. This exploits the fact that the Higgs has spin zero. Figure 9 shows that both WW and Drell-Yan are reduced, while maintaining 90% of signal.

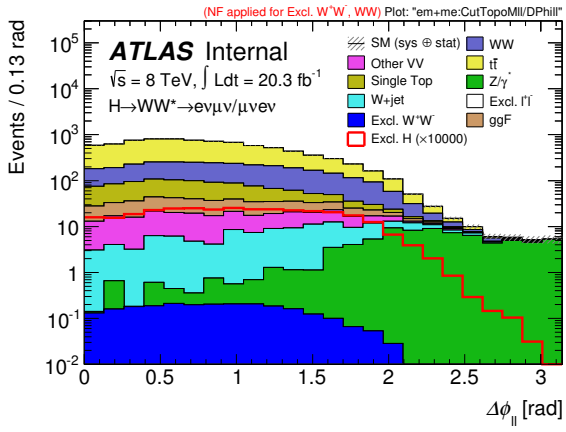

Figure 9: $\Delta\phi_{ll}$distribution. The $\Delta\phi_{ll} < 1.8$ cut reduces Drell Yan and WW backgrounds while keeping 90% of signal.

Cut	Excl. H	ggF H	WW	Excl. W^+W^-
Scale factors	NF = 100.00			
blinding	6.99 ± 0.05	585.63 ± 1.00	11641.95 ± 18.53	6.49 ± 0.03
lepton p_T 25, 15 GeV	4.59 ± 0.04	434.84 ± 0.86	10657.89 ± 17.79	5.84 ± 0.03
OS leptons	4.59 ± 0.04	434.23 ± 0.86	10618.52 ± 17.76	5.82 ± 0.03
$m_{\ell\ell} > 10$ GeV	4.52 ± 0.04	430.02 ± 0.86	10606.74 ± 17.75	5.82 ± 0.03
$E_T^{miss}, E_{T,rel}^{miss} > 20, 25$ GeV	4.27 ± 0.04	358.80 ± 0.78	8494.57 ± 15.88	5.23 ± 0.03
$\Delta\phi_{\ell\ell,MET} > 1.57$	4.27 ± 0.04	318.16 ± 0.74	7590.42 ± 15.01	5.22 ± 0.03
$p_{T,\ell\ell}$ >30 GeV	3.83 ± 0.04	285.01 ± 0.70	6183.69 ± 13.54	4.63 ± 0.03
$m_{\ell\ell} < 55$ GeV	3.28 ± 0.03	246.08 ± 0.65	1578.43 ± 6.80	0.81 ± 0.01
$\Delta\phi_{\ell\ell} < 1.8$	2.98 ± 0.03	231.26 ± 0.63	1462.57 ± 6.54	0.77 ± 0.01
Exclusivity Cuts				

Table 2: Signal selection criteria. *Blinding* refers to all the pre-selection cuts. Yields are normalized to 20.3fb^{-1}and signal is scaled by a normalization/scale factor (NF) of 100.

Table 2 summarizes the selection criteria for signal events. Signal, ggF and WW yields are estimated at each cut level. *Blinding* refers to all the pre-selection cuts. The rest of the cuts listed in the table are self-explanatory. Additional exclusivity cuts are imposed on Higgs-like events to select exclusive Higgs events. These will be discussed in Section **??**. Signal yields have been scaled by 100.

4 Exclusivity

With the high pileup environment in 8 TeV data it is crucial to improve on what has been done with 7 TeV data [4] [5] [6]. With 8 TeV data, the strategy adopted at 7 TeV of requiring a 2-track vertex and not having another track within 3 mm is only 30% efficient. This strategy is unreliable because the vertexing algorithms can be overly enthusiastic about associating tracks to a vertex. As a result, originally 2-track vertices are assigned 3 or more tracks.

4.1 Strategy

The strategy used at 8 TeV is to demand that the lepton pair not have any tracks other than those from the two leptons within a window in z_0 along the beamline. Tracks are taken from the trk container and required to have at least 1 pixel hit and at least 4 sct hits. In contrast, lepton tracks are taken from the lepton containers. It is therefore necessary to match the lepton tracks to two tracks from the trk container. For a track in the trk container to be considered a match to a lepton track it is required to be within 0.01 in ΔR and within 1 mm in z_0, with respect to the beamline. The tracks in the electron or muon containers are obtained using algorithms (GSM) different from the algorithms used in the trk container. For this reason, a lepton track may not be matched to a track in the trk container or may be matched to multiple tracks in the trk container. Figure 10 shows the number of tracks from the trk container that match the leading lepton in the event. The distribution on the left is for matching tracks to an electron and that on the right is for matching tracks to muons.

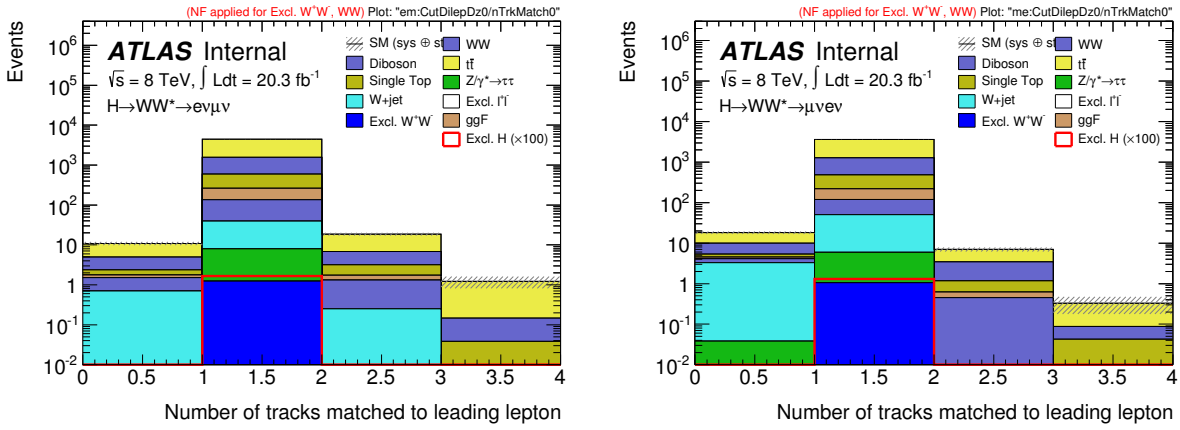

Figure 10: Number of tracks from the trk container that are matched to the leading lepton tracks. [Left] The leading lepton is an electron. [Right] The leading lepton is a muon.

Because electrons undergo bremsstrahlung more frequently than muons, there are more tracks matched to electrons than to muons. All the tracks matched to a lepton are therefore considered to be brehming from that lepton.

The exclusivity cut depends on how far in z_0 the closest unmatched track is from the lepton track pair. Figure 11 illustrates how this is quantified. The two lepton tracks are first required to be within 1 mm in z_0 to ensure that they indeed are from the lepton pair. The average z_0 position computed from the individual lepton track z_0's is considered the dilepton vertex. The distance of the closest unmatched track Δz_1 is the exclusivity variable that is cut on. Figure 12 shows Δz_1 for signal and several backgrounds. The signal is scaled by a factor of 100 to make it visible because it is heavily dominated by the backgrounds. The Δz_1 distribution in signal and other exclusive processes is characterized by a tail more spread out than in inclusive processes. Several values of Δz_1 were tried to maximize $signal/\sqrt{background}$. Figure 13

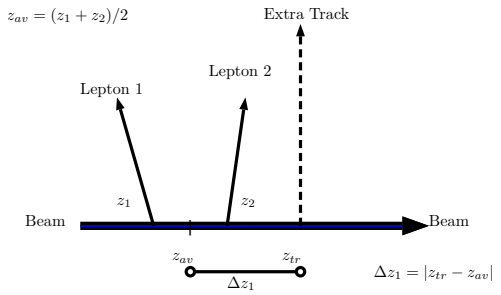

Figure 11: Illustration of the exclusivity variables.

shows $signal/\sqrt{background}$ for four values of Δz_1. This analysis settles on $\Delta z_1 > 1mm$ as the optimal exclusivity cut.

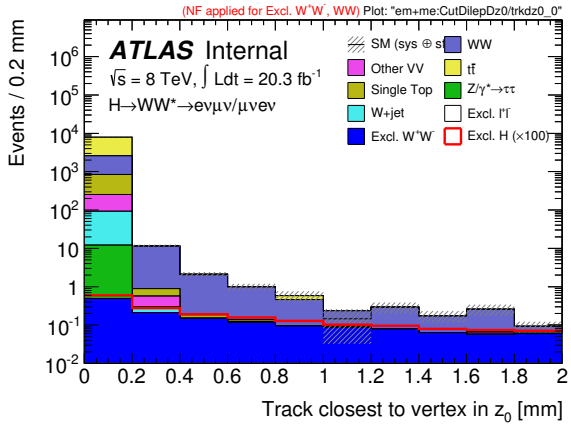

Figure 12: The main exclusivity variable Δz_1, which is the distance of the closest unmatched track to the dilepton vertex in z_0. Signal is scaled by 100. Δz_1 has a longer tail in exclusive processes compared to inclusive processes. This distrinction is exploited in this study.

4.2 Performance in data

A region in data that is rich in $Z \to \tau\tau$ events is used to validate the exclusivity selection criteria. This region follows the control region used in Ref. [12] to constrain $Z \to \tau\tau$+0-jets events in the $H \to WW^* \to \ell^+\ell^-$ study. In this study we apply it to any jet multiplicity. The selection is similar to the signal selection criteria except the following: m_{ll} region is expanded to cover $10 < m_{ll} < 80$GeV, p_T^{ll} is changed to $p_T^{ll} < 30$GeV. There is no $\Delta\phi_{ll}$ cut. Figure 14 shows some kinematic distributions of events in this $Z \to \tau\tau$ region. Before exclusivity, MC over-estimate $Z \to \tau\tau$ yields by 0.3% in this region. After exclusivity MC over-estimate the yield by 387%. This is because MC mismodeles the underlying event. Table 4.2 shows the event yields in both data and MC. Figure 14 shows key kinematic distributions before exclusivity is imposed in this control region. The good agreement between data and MC testify to the purity of the $Z \to \tau\tau$ events in data.

Figure **??** shows distributions for exclusivity variables before the exclusivity cut is imposed. The difference in z_0 between the two lepton tracks is also affected by the underlying event. The Δz_1 distribution shows a uniform disagreement between data and MC for $\Delta z_1 > 1$ mm. This disagreement results in the 387% data/MC disagreement alluded to in the preceding paragraph. To correct for this we introduce a correction factor,

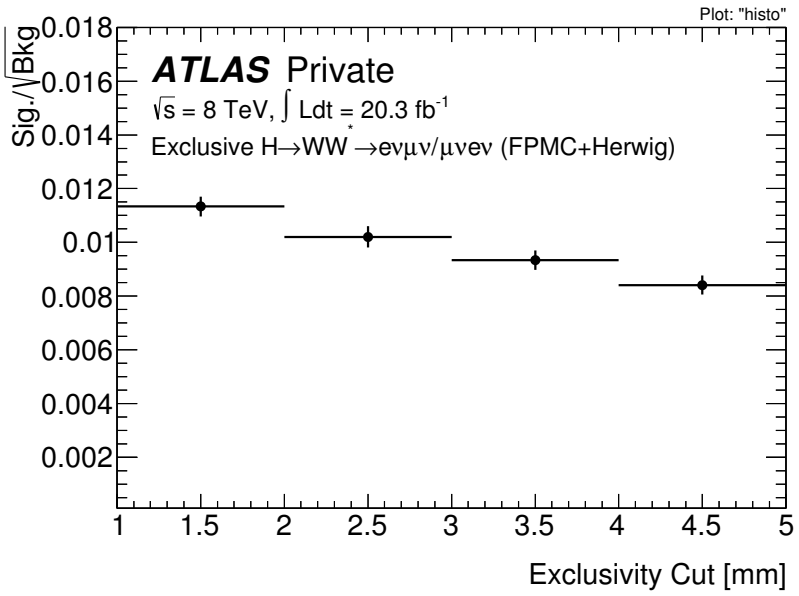

Figure 13: $signal/\sqrt{background}$ for 4 values of Δz_1. This analysis settles on $\Delta z_1 > 1mm$ as the optimal exclusivity cut.

	$Z+\gamma$/jets	Observed	Data/MC
blinding	34360.39 ± 473.93	92352	1.19 ± 0.01
lepton p_{T}	17990.93 ± 346.30	62517	1.12 ± 0.01
OS leptons	17821.85 ± 344.56	60072	1.10 ± 0.01
$m_{\ell\ell} > 10$ GeV	17803.29 ± 344.32	60002	1.10 ± 0.01
$E^{\mathrm{miss}}_{\mathrm{T,rel}} < 25$ GeV	13722.36 ± 300.23	28896	1.08 ± 0.01
$\Delta\phi_{\ell\ell,MET} > 1.57$	11127.20 ± 270.22	19390	1.04 ± 0.02
$p_{\mathrm{T},\ell\ell}$ <30 GeV	10908.72 ± 267.29	12060	0.98 ± 0.02
$m_{\ell\ell} < 80$ GeV	10651.88 ± 264.46	10600	0.95 ± 0.02
$\Delta z^0_{ll} < 1.0$ mm	10576.86 ± 263.56	10538	0.95 ± 0.02
1 mm Exclusive	58.38 ± 19.86	12	0.21 ± 0.09

Table 3: $Z \to \tau\tau$ yields in the $Z \to \tau\tau$ control region. Right before exclusivity is imposed, MC over-estimate $Z \to \tau\tau$ yields by 0.3%. After exclusivity, the over-estimation rises to 387%.

$$\text{MC Exclusivity Correction Factor, MF} = \frac{N^{mc}_{after\ excl.}/N^{mc}_{before\ excl.}}{N^{data}_{after\ excl.}/N^{data}_{before\ excl.}} \tag{3}$$

which is the ratio of the exclusivity cut efficiency in MC to its efficiency in data. Ideally it is 1.0 if MC models the underlying event correctly. An MF larger than 1.0 implies that MC over-estimate events that pass the exclusivity cut. The Alpgen+Jimmy MC that we use for this region give $MF = 4.72$.

Studies similar to the $Z \to \tau\tau$ study were done using $Z \to \mu\mu$ events, estimating them with several MC listed in Table 4. The resulting MFs are listed in the same table. All MC studied tend to over-estimate events that pass the exclusivity cut. Of all these MC, Sherpa over-estimates the most. Figure 16 shows the number of tracks within a 1.0 mm around the di-muon vertex, computed as shown in Figure 11. The exclusivity cut select only the events that are in the first bin of these plots. Clearly Sherpa over-estimates these events by a factor close to 10 (9.23 to be precise). Because this analysis relies heavily on MC to estimate major backgrounds, it is necessary to correct the MC using MFs. By comparing the

	$Z \to \mu\mu$	$Z \to \tau\tau$
Sherpa	9.23	
AlpgenPythia	1.65	
AlpgenJimmy	4.36	4.72
PowhegPythia	2.35	

Table 4: MFs obtained from studying $Z \to \mu\mu$ and $Z \to \tau\tau$ events and estimating them using several MC. Sherpa mismodels the underlying event the worst. We use Alpgen+Jimmy MC in this analysis.

Alpgen+Jimmy MF obtained using $Z \to \mu\mu$ events to the one obtained using $Z \to \tau\tau$ events we notice that they agree within 8%. Clearly the MF is a major source of systematic uncertainties. We will discuss these in Section 6.

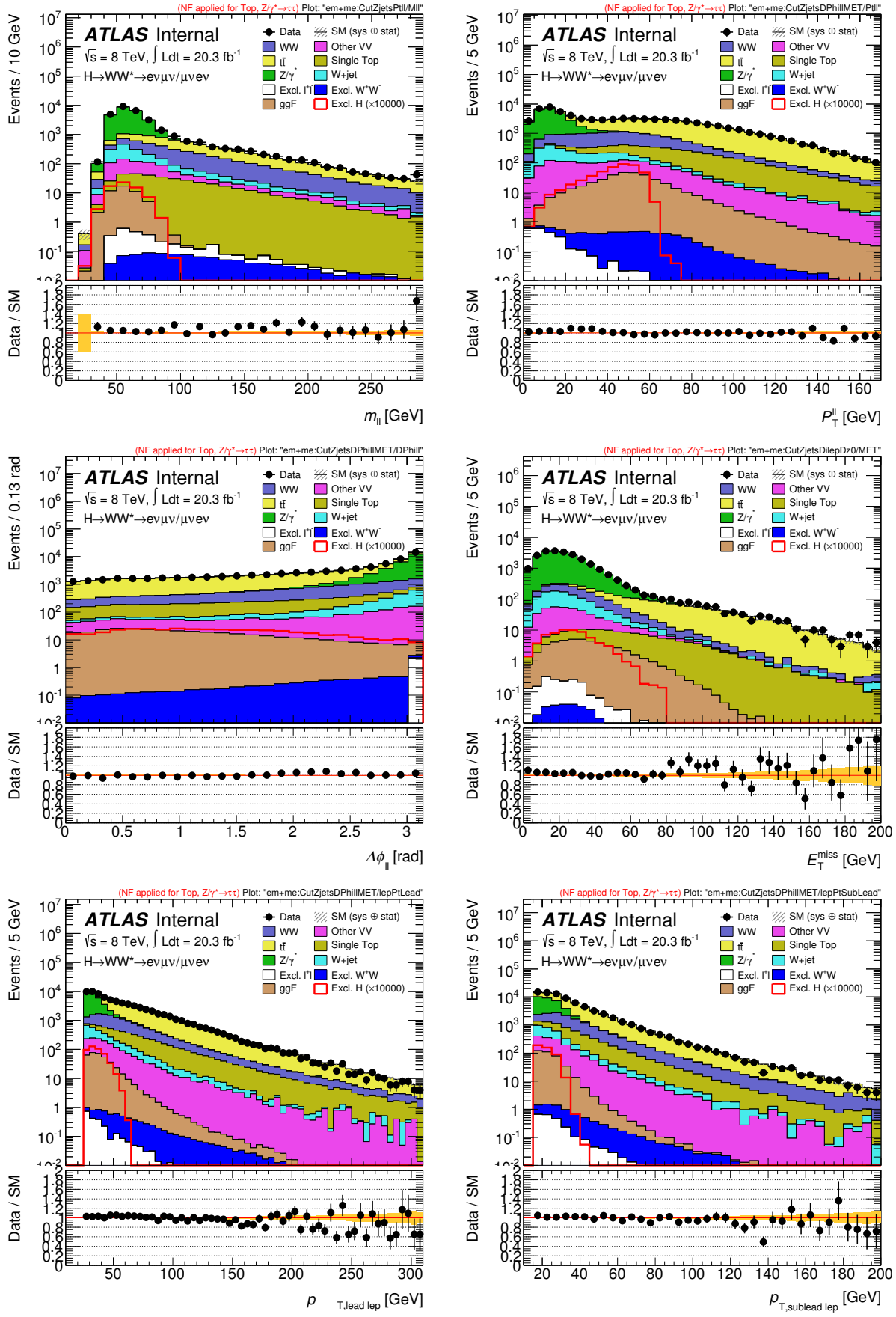

Figure 14: Key kinematic distributions in the $Z \to \tau\tau$ control region before the exclusivity cut is imposed.

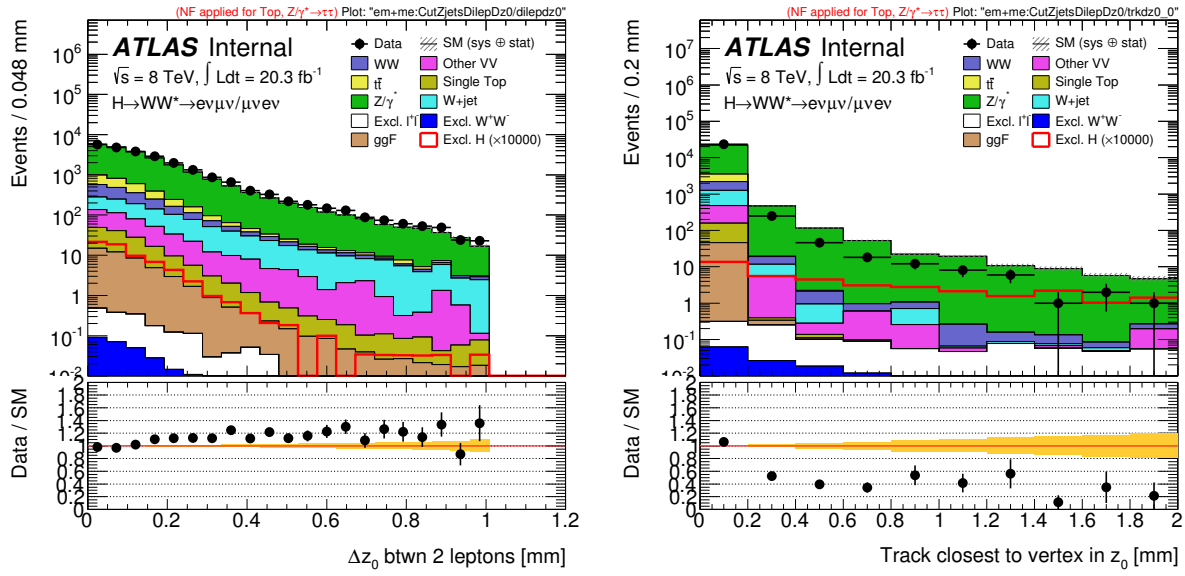

Figure 15: Exclusivity variables in the $Z \to \tau\tau$ control region show a disagreement between data and MC. This motivates the use of a correction factor on the MC.

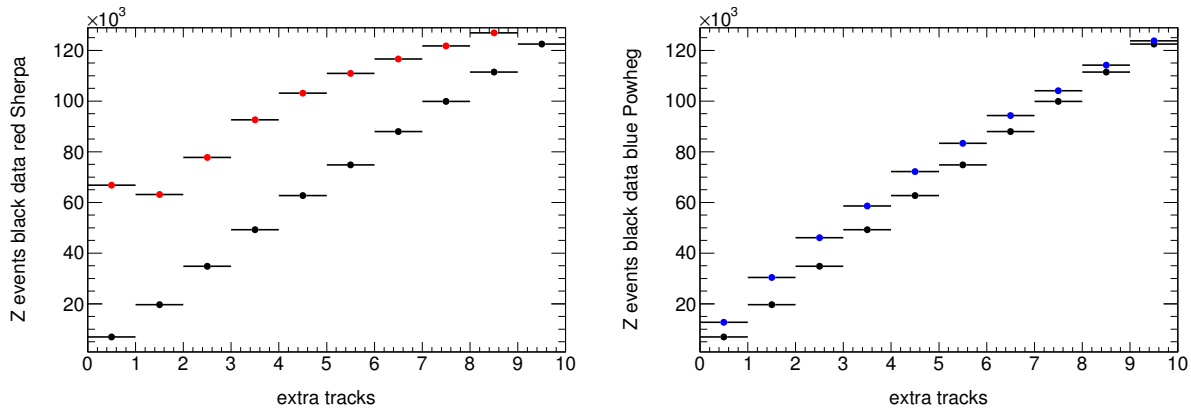

Figure 16: Number of extra tracks within a 1.0 mm window around the di-muon vertex calculated as shown in Figure 11. Events that pass exclusivity cut are in the first bin of these plots. Sherpa clearly is the worst at modelling the underlying event.

	Count
Observed	234
Predicted Elastic ll	72.0
MF-Scaled Drell-Yan	16.2
MF-Scaled Inclusive WW	0.4
MF-Scaled Exclusive WW	0.82
Flux Factor	2.99 ± 0.21

Table 5: Results for the flux factor study on exclusive di-muons. A large flux factor implies that the contribution of SD and DD processes is non-negligible.

5 Background Estimation

5.1 Exclusive WW

As shown at the end of Section 2 there are three diagrams that contribute to the exclusive WW process. Although Herwig++ models the purely elactic events well, there are no MC that model SD and DD processes. To estimate the SD and DD contributions we study di-muon events in data that pass the exclusivity cut and that have $m_{ll} > 160$ GeV to reduce di-muons from WW decays and Drell-Yan. The remaining Drell-Yan contribution in this region is estimated with MC and subtracted. All other backgrounds are considered as well but the major contributions are observed to be from inclusive WW, exclusive WW and Drell-Yan. Inclusive WW and Drell-Yan estimations are scaled with appropriate MFs to account for the MC mismodelling of the underlying event. There is no need to apply MF to exclusive WW and exclusive di-muon estimates because there is no underlying event in these processes.

After all the backgrounds are subtracted the remaining events are a good estimation of the sum of purely elastic, single dissociative and double dissociative di-muons. We introduce the

$$\text{Flux Factor} = \frac{N_{data} - N_{DY,etc}}{N_{elastic}} \tag{4}$$

which quantifies the SD and DD contributions. Detailed studies concerning this factor can be found in Ref [4]. A flux factor of 1.0 indicates that there is negligible SD and DD contributions to the exclusive di-muons. Table 5 shows the results of studying di-muon events in data. A flux factor of 2.99 ± 0.21 is obtained, in which the uncertainty is only statistical. This shows that the SD and DD contributions are non-negligible.

The diagrams that contribute to exclusive di-leptons are identical to the diagrams that contribute to exclusive WW. Thus, we can use the flux factor obtained from the di-muon study to estimate the SD and DD contributions in exclusive WW. We scale the Herwig++ estimation with 2.99 to get the expected final exclusive WW yield, which turns out to be 1.25 ± 0.02.

5.2 Inclusive WW

Inclusive WW are estimated using MC listed in Table 1. A control region is used to assess the performance of these MC. The control region is defined as follows: Events that pass all the signal region cuts up to the $p_T^{ll} > 30$ GeV cut are required to have $55 < m_{ll} < 110$ GeV and $\Delta\phi_{ll} < 2.6$ and have no jets. The 0-jet requirement suppresses $t\bar{t}$ contribution. These selection criteria for this region are similar to the 0-jet WW control region detailed in Ref. [12]. We notice that it is necessary to scale WW MC estimate by a factor of 1.22 to achieve data/MC agreement. This factor was also introduced in the $H \to WW^* \to l\nu l\nu$ studies in Ref. [12]. The exclusivity cut is then imposed after all these requirements are fulfilled and the scale factor has been applied. Figure 17 shows key kinematic distributions in this control region after scaling MC with 1.22. Table 6 shows the corresponding MC estimated yields and observed event yields.

Cuts	WW	Excl. W^+W^-	Other Bkgs	Total Bkg.	Observed	Data/MC
WW CR [$55 < m_{\ell\ell} < 110$ GeV,$\Delta\phi_{\ell\ell} < 2.6$]	2755.90 ± 9.99	1.48 ± 0.02	9750.32 ± 153.94	12513.27 ± 154.26	12176	0.97 ± 0.01
0 jet	1946.03 ± 8.42	4.35 ± 0.05	795.62 ± 133.21	2750.17 ± 133.47	2644	0.96 ± 0.05
1 mm Exclusive	1.21 ± 0.14	2.39 ± 0.03	0.47 ± 0.32	4.07 ± 0.35	9	2.21 ± 0.76

Table 6: Estimated and observed events in the WW CR.

Figure 18 shows the Δz_1 distribution after applying the 1.22 scale factor on the inclusive WW, an MF on the inclusive WW and a flux factor on the exclusive WW processes.

The inclusive WW contribution to the signal region turns out to be 0.77 ± 0.10 events.

5.3 Other Backgrounds

The rest of the backgrounds are estimated using MC, except for the W+jets. Events are selected in data that have exactly two leptons, one tightly identified and the other loosely but not tightly identified. These events turn out to be 85% W+jets. All other backgrounds are subtracted from this data sample to obtain a better estimation of the W+jets in data. All the backgrounds that use MC are applied appropriate MFs except for exclusive dileptons. A flux factor of 2.99 is applied to the exclusive dileptons estimate, which only estimates purely elastice processes. A list of all the MC generators used are listed in Table 1. We estimate 0.10 ± 0.06 from all these backgrounds.

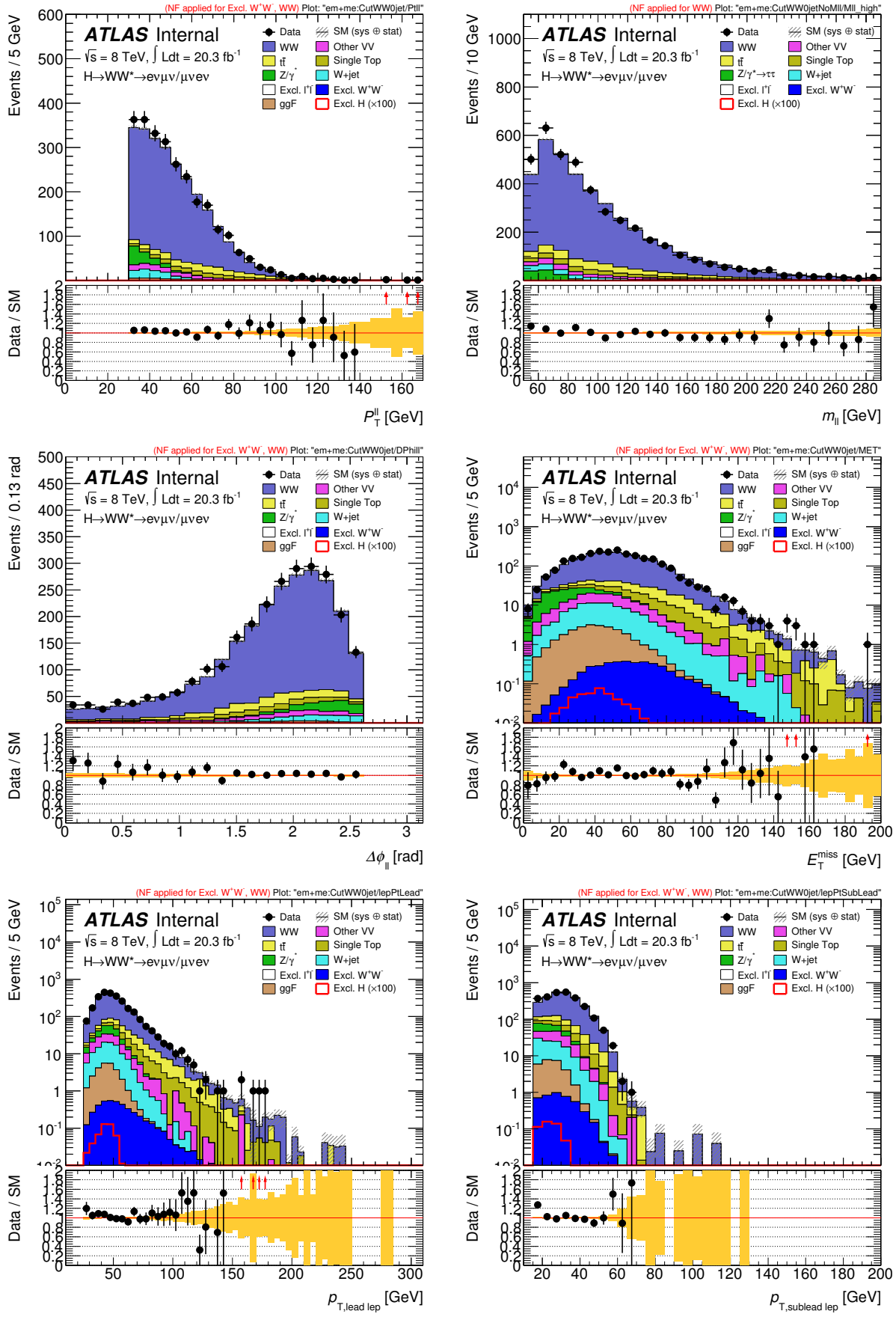

Figure 17: Key kinematic distributions in the WW control region before the exclusivity cut is imposed.

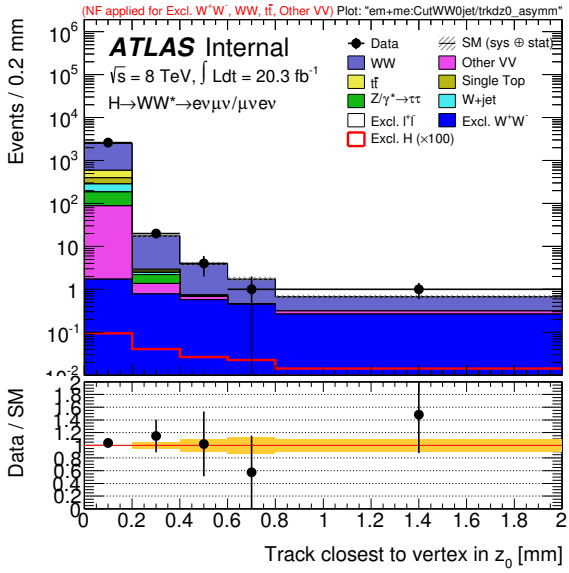

Figure 18: Exclusivity variable Δz_1 after an MF has been applied on the inclusive WW process, and a flux factor has been applied on the exclusive WW process.

HSG3	Exclusive
Electron energy Scale	MF Extrapolation
Muon energy Scale	Flux Factor
Jet energy Scale	
Jet energy resolution	
Electron resolution	
Muon resolution	

Table 7: Sources of systematic uncertainties that are currently being evaluated. Uncertainties from exclusivity variables are expected to be the most dominant.

6 Systematic Uncertainties

The majority of sources for systematic uncertainties are shared by the search the Higgs through $H \rightarrow WW^* \rightarrow lvlv$ process. Additional sources of uncertainties are from the exclusivity cuts, specifically from calculating the MF and the flux factor. The systematic uncertainties from the exclusivity variable are expected to be the largest. Table 7 shows a list of sources that are currently being evaluated.

Cuts	Inclusive WW	Exclusive W^+W^-	Other Bkgs	Total Bkg.	Excl. H [Signal]
Scale factors					NF = 100.00
$\Delta\phi_{\ell\ell} < 1.8$	1779.36 ± 7.96	2.31 ± 0.03	6783.23 ± 227.73	8570.49 ± 227.87	2.98 ± 0.03
$\Delta z^0_{ll} < 1.0$	1776.68 ± 7.95	2.31 ± 0.03	6774.47 ± 227.72	8559.04 ± 227.86	2.98 ± 0.03
1 mm Exclusive	0.70 ± 0.10	1.25 ± 0.02	0.10 ± 0.06	2.05 ± 0.12	1.62 ± 0.02

Table 8: Main contributions to signal region contamination are inclusive WW and exclusive WW

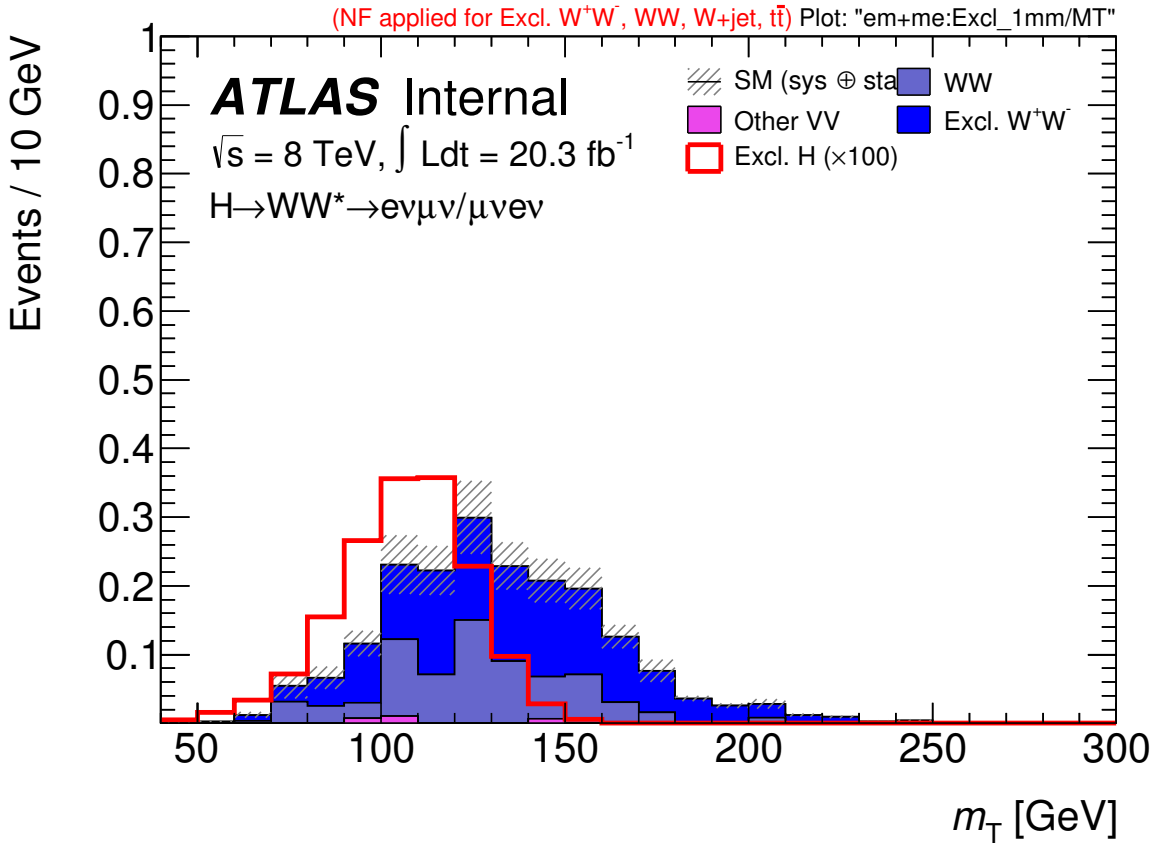

Figure 19: m_T for events expected in the signal region. The major backgrounds expected are exclusive and inclusive WW.

7 Results

Table 8 summarizes the expected event yields from signal and background. Signal has been scaled by a factor of 100 for visibility. Figure 19 shows the m_T distribution for events in the signal region. The major backgrounds are the exclusive and inclusive WW.

An expected limit on the exclusive Higgs cross section was computed from these results. The only systematic uncertainty included in the calculation was on the integrated luminosity. The result of the fit is therefore statistical. Systematic uncertainties are currently being evaluated and the expected limit is under constant modification. Table 9 shows the current results of the limit on the exclusive higgs cross section with the branching ratio factored in. This corresponds to a limit on the total production cross-section of 770 fb on the exclusive higgs. Compare this value with 3 fb predicted by the KMR model.

Cut	Limit [pb]	$+1\sigma$	$+2\sigma$	-1σ	-2σ
1 mm	0.010	0.015	0.024	0.007	0.006

Table 9: Limits set on $\sigma \times BR(H \rightarrow WW \rightarrow lvlv)[pb]$ 95% CL using a 1-bin fit on m_T. The only systematic uncertainty considered is from integrated luminosity.

8 Summary

Studies on the exclusive higgs could provide a very clean channel to further study properties of the higgs boson. It is therefore important to quantify the production cross section of this process with the current available data that corresponds to LHC's 8 TeV collision energy. Previous analyses that studied exclusive processes have exploited the existence of rapidity gaps and used reconstructed vertices with their associated tracks to devise exclusivity selection criteria. These techniques are not as efficient with pileup that results from the 8 TeV collision energy.

In this analysis the exclusive Higgs was searched for in the $H \rightarrow WW^* \rightarrow lvlv$ decay channel. Exclusivity selection criteria that are dependent on the two lepton tracks were developed. These criteria are sensitive to pileup and are expected to become ineffective with high pile up in Run II, at 13 TeV collision energy. The major backgrounds to exclusive $H \rightarrow WW^* \rightarrow lvlv$ are the inclusive and exclusive WW. All other backgrounds were considered but have very low contributions to the signal region. A limit on the total production cross section of 770 fb was obtained for the exclusive Higgs. This shows that this analysis is not sensitive to the KMR model for the exclusive Higgs, which predicts 3 fb at 8 TeV.

Systematic uncertainties are currently being evaluated and the quoted limit is also being updated.

References

[1] V. A. Khoze, A. D. Martin, and M. Ryskin, *Higgs or dijet production in double rapidity gap events*, arXiv:hep-ph/0006005 [hep-ph].

[2] V. A. Khoze, A. D. Martin, and M. Ryskin, *Can the Higgs be seen in rapidity gap events at the Tevatron or the LHC?*, Eur.Phys.J. **C14** (2000) 525–534, arXiv:hep-ph/0002072 [hep-ph].

[3] R. Staszewski, P. Lebiedowicz, M. Trzebinski, J. Chwastowski, and A. Szczurek, *Exclusive $\pi^+\pi^-$ Production at the LHC with Forward Proton Tagging*, Acta Phys.Polon. **B42** (2011) 1861–1870, arXiv:1104.3568 [hep-ex].

[4] CMS, *Exclusive photon-photon production of muon pairs in pp collisions at $\sqrt{s} = 7$ TeV*, JHEP **01** (2012) .

[5] CMS, *Search for exclusive or simi-exclusive photon pair production and observation of exclusive and semi-exclusive electron pair production in pp collisions at $\sqrt{s} = 7$ TeV*, JHEP **11** (2012) .

[6] *Monte Carlo studies of two-photon production of muon pairs*, Tech. Rep. ATL-COM-PHYS-2013-1479, October, 2013.

[7] V. Khoze, A. Martin, and M. Ryskin, *Prospects for new physics observations in diffractive processes at the LHC and Tevatron*, Eur.Phys.J. **C23** (2002) 311–327, arXiv:hep-ph/0111078 [hep-ph].

[8] J. Cudell, A. Dechambre, O. Hernandez, and I. Ivanov, *Central exclusive production of dijets at hadronic colliders*, Eur.Phys.J. **C61** (2009) 369–390, arXiv:0807.0600 [hep-ph].

[9] A. D. Martin and M. Ryskin, *Unintegrated generalized parton distributions*, Phys.Rev. **D64** (2001) 094017, arXiv:hep-ph/0107149 [hep-ph].

[10] Y. Dokshitzer, D. Dyakonov, and S. Troyan, *Hard processes in quantum chromodynamics*, Physics Reports **58** (1980) no. 5, 269 – 395.

[11] V. A. Khoze, A. D. Martin, and M. Ryskin, *Soft diffraction and the elastic slope at Tevatron and LHC energies: A MultiPomeron approach*, Eur.Phys.J. **C18** (2000) 167–179, arXiv:hep-ph/0007359 [hep-ph].

[12] *Observation and measurement of Higgs boson decays to WW^* with ATLAS at the LHC*, Tech. Rep. ATLAS-CONF-2014-060, CERN, Geneva, Oct, 2014.

[13] A. Collaboration, *https://atlas-lumicalc.cern.ch/*, .

[14] ATLAS Collaboration, G. Aad et al., *Measurement of the muon reconstruction performance of the ATLAS detector using 2011 and 2012 LHC proton-proton collision data*, Eur.Phys.J. **C74** (2014) no. 11, 3130, arXiv:1407.3935 [hep-ex].